BJP BRITISH JOURNAL OF PHARMACOLOGY
BPS BRITISH PHARMACOLOGICAL SOCIETY

BJP British Journal of Pharmacology

DOI:10.1111/j.1476-5381.2010.00945.x
www.brjpharmacol.org

RESEARCH PAPER

PM01183, a new DNA minor groove covalent binder with potent *in vitro* and *in vivo* anti-tumour activity

JFM Leal[1], M Martínez-Díez[1], V García-Hernández[2], V Moneo[1], A Domingo[2], JA Bueren-Calabuig[3], A Negri[3], F Gago[3], MJ Guillén-Navarro[1], P Avilés[1], C Cuevas[1], LF García-Fernández[1] and CM Galmarini[1]

[1]*Cell Biology Department, PharmaMar SA, Spain,* [2]*Department of Biochemistry and Molecular Biology, University of Alcalá, Spain, and* [3]*Department of Pharmacology, University of Alcalá, Spain*

Correspondence
Carlos M. Galmarini, PharmaMar Cell Biology Department, Avda. de los Reyes, 1, 28770 Colmenar Viejo, Madrid, Spain. E-mail: cgalmarini@pharmamar.com

Keywords
antineoplastic agents; tetrahydroisoquinolines; DNA breaks; apoptosis

Received
15 January 2010
Revised
12 April 2010
Accepted
8 June 2010

BACKGROUND AND PURPOSE
PM01183 is a new synthetic tetrahydroisoquinoline alkaloid that is currently in phase I clinical development for the treatment of solid tumours. In this study we have characterized the interactions of PM01183 with selected DNA molecules of defined sequence and its *in vitro* and *in vivo* cytotoxicity.

EXPERIMENTAL APPROACH
DNA binding characteristics of PM01183 were studied using electrophoretic mobility shift assays, fluorescence-based melting kinetic experiments and computational modelling methods. Its mechanism of action was investigated using flow cytometry, Western blot analysis and fluorescent microscopy. *In vitro* anti-tumour activity was determined by 3-(4,5-dimethylthiazol-2-yl)-2,5-diphenyltetrazolium bromide assay and the *in vivo* activity utilized several human cancer models.

KEY RESULTS
Electrophoretic mobility shift assays demonstrated that PM01183 bound to DNA. Fluorescence-based thermal denaturation experiments showed that the most favourable DNA triplets providing a central guanine for covalent adduct formation are AGC, CGG, AGG and TGG. These binding preferences could be rationalized using molecular modelling. PM01183–DNA adducts in living cells give rise to double-strand breaks, triggering S-phase accumulation and apoptosis. The potent cytotoxic activity of PM01183 was ascertained in a 23-cell line panel with a mean GI_{50} value of 2.7 nM. In four murine xenograft models of human cancer, PM01183 inhibited tumour growth significantly with no weight loss of treated animals.

CONCLUSIONS AND IMPLICATIONS
PM01183 is shown to bind to selected DNA sequences and promoted apoptosis by inducing double-strand breaks at nanomolar concentrations. The potent anti-tumour activity of PM01183 in several murine models of human cancer supports its development as a novel anti-neoplastic agent.

Abbreviations
CK-18, cytokeratin-18; DAPI, 4′,6-diamidino-2-phenylindole; DMSO, dimethyl sulphoxide; DSBs, double-strand breaks; ICL, interstrand crosslink; MTT, 3-(4,5-dimethylthiazol-2-yl)-2,5-diphenyltetrazolium bromide; Pol II, polymerase II; TC-NER, transcription-coupled-nucleotide excision repair

Introduction

DNA is a well-characterized intracellular target in cancer chemotherapy (Reddy *et al.*, 2001) and consists of two right-handed polynucleotide chains running in opposite directions to form a double helix. This DNA duplex is stabilized by both intra-strand stacking interactions and hydrogen bonds

between paired bases in the two strands: adenine forms two hydrogen bonds with thymine while guanine forms three hydrogen bonds with cytosine. The base pairs are rotated by 36° with respect to each adjacent pair. This structure gives rise to two well-defined clefts known as the major and minor grooves. The major groove is deep and wide while the minor groove is narrow and shallow. As a result, DNA-binding proteins and drugs usually make contacts to the sides of the bases exposed in both the major (Pabo and Sauer, 1984) and the minor grooves (Rohs *et al.*, 2009). The DNA major groove represents a site of attack for cisplatin and many alkylating agents whereas other anti-tumour drugs such as mitomycin C, chromomycin A_3 or the ecteinascidins bind to the minor groove.

Currently, there is a renewed interest in the development of molecules that target the minor groove of DNA (Susbielle *et al.*, 2005). One of the best examples is trabectedin (Yondelis®), a member of the ecteinascidin family originally derived from the marine tunicate *Ecteinascidia turbinata* that is currently used for the treatment of patients with advanced or metastatic soft tissue sarcoma and relapsed platinum-sensitive ovarian cancer. Trabectedin reacts with the exocyclic amino group of certain guanines in the minor groove of DNA (Kishi *et al.*, 1984; Guan *et al.*, 1993; Pommier *et al.*, 1996; Moore *et al.*, 1997) forming a covalent bond. The resulting adduct is additionally stabilized through the establishment of van der Waals interactions and one or more hydrogen bonds with neighbouring nucleotides in the opposite strand of the DNA double helix (Moore *et al.*, 1997; Seaman and Hurley, 1998), thus creating the equivalent to a functional interstrand crosslink (Casado *et al.*, 2008).

PM01183 (Figure 1A) is a new synthetic alkaloid structurally related to ecteinascidins (Rinehart *et al.*, 1990; Manzanares *et al.*, 2001) that is currently in phase I clinical development for the treatment of solid tumours. In common with trabectedin, PM01183 contains a pentacyclic skeleton composed of two fused tetrahydroisoquinoline rings (subunits A and B) that is mostly responsible for DNA recognition and binding but the additional module (ring C) in PM01183 is a tetrahydro β-carboline rather than the additional tetrahydroisoquinoline present in trabectedin. This structural difference may confer pharmacokinetic benefits as well as intrinsic activity. In PM01183 the C-ring, which protrudes from the DNA minor groove, has been proposed to be involved in direct interactions with specific factors of DNA repair pathways (Herrero *et al.*, 2006; Casado *et al.*, 2008). In this study we have characterized: (i) the molecular interactions between PM11083 and several DNA oligo- and polynucleotides; and (ii) the *in vitro* and *in vivo* cytotoxic activity of the compound.

The DNA binding characteristics were studied using a combination of electrophoretic mobility shift assays, fluorescence-based melting kinetic experiments and computational modelling methods. We also looked at the type of DNA damage subsequently generated in living cells as a consequence of PM01183-DNA adduct formation as well as cell cycle perturbations and type of cell death induced by this compound. Finally, the *in vitro* and *in vivo* anti-tumour activity of PM01183 was investigated using several models of human cancers.

Methods

DNA electrophoretic mobility shift assay

The binding assay was performed with a 250 bp PCR product from the human adiponectin gene (Sigma, St Louis, MO, USA). After incubation with appropriate concentrations of the compound at 25°C during 1 h, the DNA was subjected to electrophoresis in a 2% (w/v) agarose/TAE gel, stained with 1 $\mu g \cdot mL^{-1}$ ethidium bromide and photographed.

DNA melting assay

Synthetic oligodeoxynucleotides with one strand 5′-end-labelled with the fluorophore 6-carboxyfluorescein and the complementary strand 3′-end-labelled with the quencher tetramethylrhodamine were synthesized at Bonsai Technologies (Madrid, Spain) (Table S1). For the experiments, we followed the methodology previously described (Negri *et al.*, 2007; Casado *et al.*, 2008) using a 7500 Fast Real-Time PCR System (ABI Prism, Applied Biosystems, Foster City, CA, USA). Analyses of the raw data obtained for each oligodeoxynucleotide using an in-house developed Visual Basic Application running on Microsoft Excel (Microsoft, Redmond, WA, USA) yielded estimates of both the increase in melting temperature (ΔT_m) brought about by drug binding, relative to the free DNA molecule, and the ligand concentration that produces half the maximal change in melting temperature (C_{50}). The inverse of this latter value ($1/C_{50}$) was taken as a measure of the relative DNA binding affinity, and the parameter $\Delta T_m(max)$ was used to reflect the relative stability of the DNA–ligand complexes (Negri *et al.*, 2007).

Computational methods

Molecular modelling and simulation methods were used to study in atomic detail: (i) the binding orientation required to activate dehydration of the

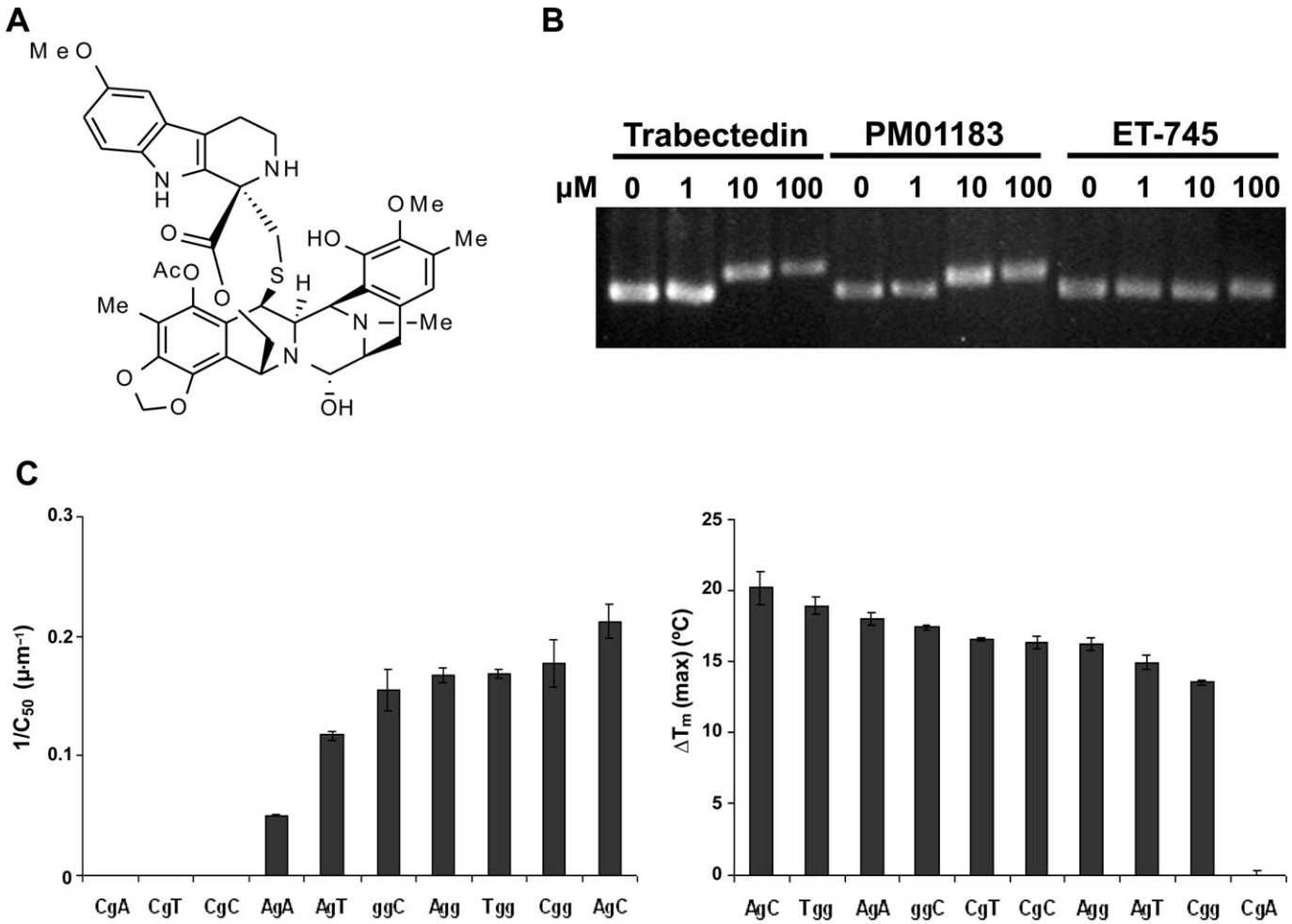

Figure 1

Chemical structure and DNA binding properties of PM01183. (A) Structure of PM01183; (B) binding to naked DNA. Drugs were incubated with a 250 bp PCR product at 25°C during 1 h and the electrophoresis was run in 2% agarose-TAE; (C) relative binding affinities for different DNA triplet sequences. PM01183 was incubated with the labelled double-strand oligodeoxynucleotides at 25°C during 1 h; then the melting assay was started in a 7500 Fast Real-Time PCR System by increasing the temperature up to 95°C in small steps of 1°C·min^{-1}. Analysis of the $1/C_{50}$ parameter (drug affinity for specific DNA sequences) and ΔT_m(max) (stability of the drug–DNA complex) were analysed with an in-house developed Visual Basic Application (VBA) running on Microsoft Excel. The values correspond to the mean and standard deviation from at least two independent experiments for each sequence.

carbinolamine and promote the nucleophilic attack by the amino group to a central guanine in a favoured DNA triplet; and (ii) the consequences of covalent adduct formation in the minor groove. To this end, a pre-covalent complex between PM01183 and an oligonucleotide of sequence 5′-d(CAATACG GATAAG)/5′-d(CTTATCCGTATTG), containing a central CGG as a target site, was built as previously reported for trabectedin (Marco *et al.*, 2006). The covalent complex with the underlined guanine was similarly built and both complexes were then refined in the presence of explicit solvent and counterions using energy minimization techniques in the AMBER force field (Case *et al.*, 2005). The stabilities and geometrical features of the complexes were studied by means of 20 ns of unrestrained molecular dynamics simulations using the same conditions as described previously.

Cell culture and cytotoxicity

All the tumour cell lines used in this study were obtained from the American Type Culture Collection (ATCC, Rockville, MD, USA). For the cytotoxicity experiments, cells were seeded in 96-well trays. Serial dilutions of PM01183 dissolved in dimethyl sulphoxide (DMSO) were prepared and added to the cells in fresh medium, in triplicate. Exposure to the drug was maintained during 72 h and cellular viability was estimated from conversion of 3-(4,5-dimethylthiazol-2-yl)-2,5-diphenyltetrazolium

bromide (MTT) (Sigma, St Louis, MO, USA) to its coloured reaction product, MTT formazan, which was dissolved in DMSO so as to measure absorbance at 540 nm with a POLARStar Omega Reader (BMG Labtech, Offenburg, Germany). Determination of the concentration giving 50% growth inhibition (GI_{50}) values was performed by iterative non-linear curve fitting using the Prism 5.0 statistical software (GraphPad, La Jolla, CA, USA). The data presented are the average of three independent experiments performed in triplicate.

Fluorescent microscopy

Cells were treated with the appropriate concentration of PM01183 for 6 h, washed and then cultured for 18 additional hours. At the end of this period, they were fixed (4% paraformaldehyde), permeabilized (0.5% Triton X-100) and incubated with the primary anti-γ-H2AX monoclonal antibody (Upstate, Temecula, CA, USA) for 1 h at 37°C. Thereafter the cells were washed and incubated with the AlexaFluor 594 secondary goat anti-mouse IgG (Invitrogen, Carlsbad, CA, USA) for 30 min at 37°C. Finally, the slides were incubated with Hoechst 33 342 (Sigma, St Louis, MO, USA) and mounted with Mowiol mounting medium. Pictures were taken with a Leica DM IRM fluorescence microscope equipped with a 100× oil immersion objective and a DFC 340 FX digital camera (Leica, Wetzlar, Germany).

Cell cycle analysis

For the cell cycle experiments and sub-G_1 peak determination, cells were treated with the appropriate amount of PM01183 for 12 h and 24 h, and then stained with 0.4 $\mu g \cdot mL^{-1}$ propidium iodide. Samples were analysed with a FACScalibur flow cytometer (Beckton and Dickinson, Franklin Lakes, NJ, USA) and the FlowJo7 cytometry analysis software.

Apoptosis detection

For the chromatin condensation assay, cells were treated with the appropriate amount of the compound for 24 h and stained with 4′,6-diamidino-2-phenylindole (DAPI). Chromatin condensation in early apoptotic cells was assessed with a DM IRM microscope (Leica, Wetzlar, Germany). For the M30-Apoptosense® solid-phase sandwich enzyme immunoassay (Peviva, Bromma, Sweden), the kit instructions were followed. Briefly, cells were exposed to the appropriate concentration of the drug for 24 h. Cell lysates were obtained, transferred to an assay well and incubated for 4 h following addition of a mouse monoclonal (M30) antibody-horseradish peroxidase (HRP) conjugate. Once the antigen-M30 was bound to the M5-coated surface of the wells, they were extensively washed and incubated with the 3,3′,5,5′-tetramethyl-benzidine substrate in the dark for 20 min. Finally, the reaction was ended by addition of a stop solution and the plates were read at 450 nM within 30 min on a Victor3 platform (Perkin Elmer).

Western blot assays

For immunoblotting, cells were treated with the appropriate compound concentration for 24 h and lysed with RIPA lysis buffer. Protein content was determined by the modified Bradford method. Samples were separated in 7.5% SDS-PAGE, transferred onto an Immobilon-P membrane. Then, membranes were incubated with the appropriate primary antibody for 1 h, washed and incubated with the secondary antibody. Finally, protein was visualized using the ECL System (GE Healthcare, Fairfield, CT, USA). We used an anti-poly ADP ribose polymerase (PARP) rabbit polyclonal antibody from Santa Cruz (Santa Cruz, CA, USA), and an anti-α-tubulin monoclonal antibody from Sigma (St Louis, MO, USA). Secondary antibodies were HRP-conjugated goat anti-rabbit secondary antibody (R&D Minneapolis, MN, USA) and HRP-conjugated goat anti-mouse secondary antibody (Santa Cruz, CA, USA).

Anti-tumour activity in xenograft murine models

All animal care and experimental procedures were approved by the Institutional Animal Care and Use Committee of PharmaMar, Inc. (Cambridge, MA, USA), in an AAALAC accredited animal facility. Four to 6-week-old athymic *nu/nu* mice (Harlan Sprague Dawley, Madison, WI, USA) were s.c. xenografted with NCI-H460 (lung), A2780 (ovary), HT29 (colon) and HGC-27 (gastric) cells into their right flank with *c.* 3×10^6 cells in 0.2 mL of a mixture (50:50; v:v) of Matrigel basement membrane matrix (Beckton Dickinson, Frankin Lakes, NJ, USA) and serum-free medium. When tumours reached *c.* 150 mm^3, mice were randomly assigned to treatment or control groups. PM01183 was intravenously administered in three consecutive weekly doses (0.18 $mg \cdot kg^{-1} \cdot day^{-1}$) whereas the control animals received an equal volume of vehicle with the same schedule. Caliper measurements of the tumour diameters were made twice weekly and tumour volumes were calculated according to the following formula: $(a \cdot b)^2/2$, where a and b were the longest and shortest diameters respectively. Animals were humanely killed when their tumours reached 3000 mm^3 or if significant toxicity (e.g. severe body weight reduction) was observed. Differences in tumour volumes between treated and control groups were evaluated using the Mann–

Whitney *U*-test. Statistical analyses were performed by LabCat® v8.0 SP1 (Innovative Programming Associates, Inc., NJ, USA).

Materials

PM01183 is a PharmaMar SAU proprietary drug produced by chemical synthesis. ET-745 is a synthetic ecteinascidin that lacks the carbinolamine (hemiaminal) group (Manzanares *et al.*, 2001) and does not bind covalently to DNA (David-Cordonnier *et al.*, 2005). DAPI and Z-Vad-fmk (a pan-caspase inhibitor) were purchased from Sigma (St Louis, MO, USA) (Figure S1).

Results

DNA binding properties of PM01183

The mechanism of action of PM01183 was expected to rely on the covalent reaction with selected guanines in the DNA double helix. Thus, we first investigated its binding to DNA through band shift assays that allow the qualitative assessment of the molecular weight increase brought about in this macromolecule by the covalent bonding of PM01183 to the amino group of a central guanine in well-defined DNA triplets. As positive and negative controls we used, respectively, trabectedin and ET-745, a derivative unable to form a covalent adduct with DNA because it lacks the reactive hydroxyl group making up the hemiaminal in PM01183 (Figure S1, Manzanares *et al.*, 2001). Figure 1B shows the result of a typical band shift experiment that used increasing concentrations of PM01183 to saturate the 250 bp DNA probe with the compound and give rise to an increase in molecular weight. As expected, the delay in electrophoretic migration reflected that PM01183 does indeed bind to naked DNA. In these experimental conditions, DNA saturation required ~10 μM of the compound.

The ability of PM01183 to stabilize the double helix was assessed by means of several tailor-made fluorophore-labelled oligonucleotides encompassing most of the possible DNA triplet combinations involving a central guanine (Table S1). Figure 1C summarizes the results of the DNA melting experiments. The mean ± SD $1/C_{50}$ and $\Delta T_m(max)$ values for PM01183 were 0.15 ± 0.5 μM^{-1} and 15 ± 5°C respectively. According to the affinity indicator $1/C_{50}$, the most favourable triplets for PM01183 bonding to DNA appeared to be AGC, CGG, AGG and TGG triplets whereas the highest thermal stabilities were observed for DNA adducts involving an AGC, TGG, AGA and GGC site. The lowest affinities and stabilities were observed in oligonucleotides containing CGC, CGT and CGA sites.

Molecular modelling data

The general structure of the CGG-containing pre-alkylation binding complex shows PM01183 fitting snugly within the minor groove with subunit A protruding perpendicularly to the helical axis of the DNA molecule in front of the target guanine (G7), subunit B stacking over the sugar ring of the complementary cytosine (C20), and one side of subunit C making extensive contacts with the sugar ring of the nucleotide on the 3′ side of the central triplet. The N12 proton in subunit A of PM01183 plays a clear role in sequence recognition and also mediates the *in situ* dehydration of the hemiaminal to yield the reactive iminium intermediate, as reported previously for trabectedin (Garcia-Nieto *et al.*, 2000). Thus, in our simulation of this pre-covalent complex, the protonated N12 remains hydrogen bonded to the N3 acceptor atom of G21 whereas the OH acts both as a hydrogen bond donor to O2 of C20 and as a hydrogen bond acceptor from N2 of G7 (Figure 2A, left). Conversely, the methylendioxy oxygen from subunit B that faces the minor groove is also involved in a hydrogen bond with N2 of G8. Interestingly, the double helical structure is only minimally perturbed as a result of PM01183 binding, except for widening of the minor groove and a slight bend towards the major groove.

In the covalent complex containing the PM01183-G7 adduct (Figure 2A, right), the minor groove remains widened and the major groove appears compressed in the central region due to significant increases in roll at C6/G7 and G7/G8 steps. As a result, the conformation of the DNA is slightly bent. This finding together with the facts that the minor groove is occupied and some functional groups are exposed to the solvent are likely to have an impact on the ability of this binary complex to associate or interfere with one or more DNA-binding proteins involved in transcription, replication and/or repair within the cell, not necessarily the same that are affected by trabectedin-DNA adducts.

PM01183 treatment induces double-strand DNA breaks in cancer cells and S-phase accumulation

We further assessed whether PM01183-DNA adducts could eventually give rise to double-strand breaks (DSBs) in living cells. For this purpose, we analysed the formation of γ-H2AX foci as a surrogate indicator of DSB formation. Figure 2B shows typical results found in A549 cells treated with PM01183 for 6 h at the indicated concentrations. At 5 nM, few cells showed γ-H2AX staining. In contrast, at 25 nM,

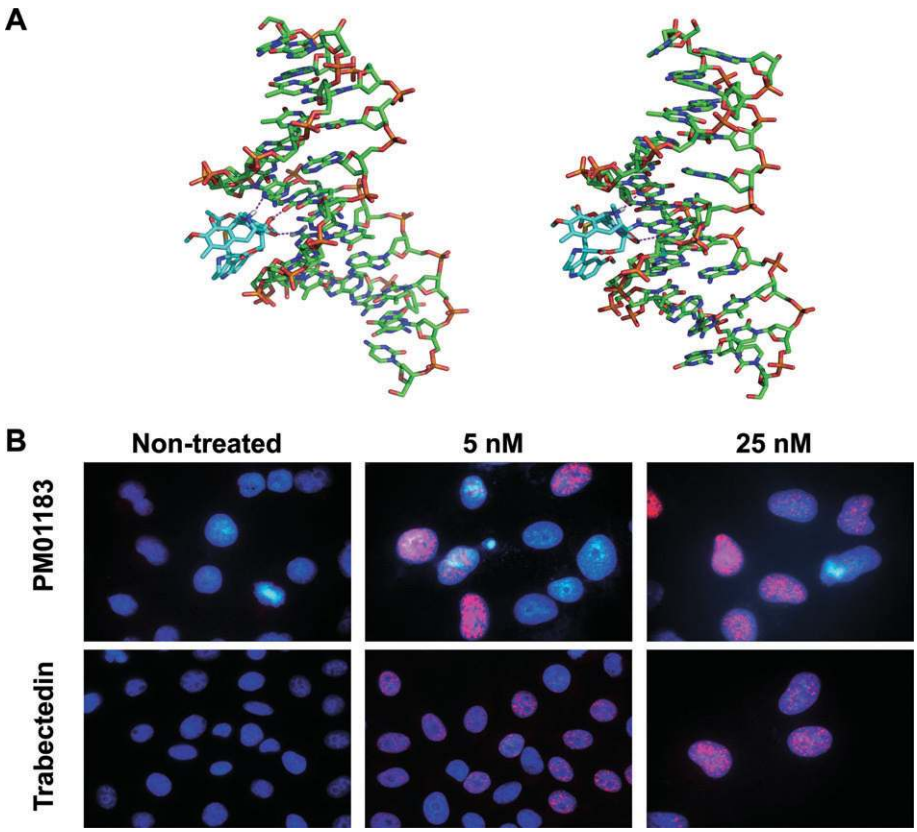

Figure 2

Modelling of DNA–PM01183 complexes and induction of DNA double-strand breaks following exposure to PM01183. (A) Refined and equilibrated molecular models of the pre-covalent (left) and covalent (right) complexes between PM01183 (C atoms in cyan) and the CGG-containing oligonucleotide (C atoms in green). The dotted lines represent hydrogen bonds. (B) A549 cells were treated with either PM01183 or trabectedin at the indicated concentrations during 6 h, followed by additional 18 h of incubation without the drug. After fixation, cells were immunostained for γ-H2AX and nuclei were visualized with Hoechst 33342.

most of the cells were stained for γ-H2AX and each of the positive cells carried a large number of foci, indicating that several DSBs per cell were induced at this drug concentration. As shown in Figure 2B, equimolar concentrations of PM01183 and trabectedin caused similar levels of DSBs.

Table 1 and Table S2 summarize the results of our assessment of possible cell cycle perturbations after 12 and 24 h of exposure to PM01183. At both time intervals, low (15 nM) and high (150 nM) drug concentrations induced an increase of the S-phase population in A549 (lung), HCT116 (colorectal), HT29 (colorectal) and MDA-MB-231 (breast) cancer cells that was more pronounced after exposure for 24 h. Of note, the S-phase accumulation was higher at 15 nM, probably due to a higher cell survival. In IGROV-1 cells, we did not observe any S-phase accumulation, most likely due to the extensive cell death induced by the compound at both concentrations after 24 h treatment (see below).

PM01183 induces cell death by apoptosis

We investigated whether exposure to PM01183 was able to induce a canonical apoptosis response in tumour cells. First, we determined whether the drug was able to generate late apoptosis by detecting the flow cytometric sub-G_1 cell population (Figure 3A, Table 1). Treatment of A549, HCT116 and HT-29 cells resulted in an increase in the sub-G_1 population at the highest concentration (150 nM). On the other hand, MDA-MB-231 cells died with a slower kinetics while IGROV-1 cells more rapidly. These data indicated that the percentage of cells entering the sub-G_1 peak after 24 h of treatment with PM01183 was cell type- and concentration-dependent. Fluorescence microscopy confirmed that exposure of the A549 cell line to 150 nM PM01183 for 24 h induced the appearance of cells with a visible apoptotic nuclear morphology including strong chromatin condensation (Figure 3B).

Table 1
Cell cycle perturbations induced by PM01183

	Cell cycle phase	Control	15 nM	150 nM
A549	Sub-G_1	3	11	28
	G_0/G_1	62	24	37
	S-phase	16	40	23
	G_2/M	19	25	12
HT29	Sub-G_1	7	8	25
	G_0/G_1	55	17	31
	S-phase	26	68	29
	G_2/M	12	7	15
HCT116	Sub-G_1	5	7	37
	G_0/G_1	59	21	36
	S-phase	17	45	14
	G_2/M	19	27	13
MDA-MB-231	Sub-G_1	3	3	3
	G_0/G_1	53	30	37
	S-phase	25	50	33
	G_2/M	19	17	27
IGROV-1	Sub-G_1	4	30	76
	G_0/G_1	53	33	9
	S-phase	20	15	9
	G_2/M	23	22	6

Cells were treated with the appropriate amount of the compound for 24 h, and then stained with 0.4 $\mu g \cdot mL^{-1}$ propidium iodide. Samples were analysed with a FACScalibur flow cytometer (Beckton and Dickinson, Frankin Lakes, NJ, USA) and the FlowJo7 cytometry analysis software. Values are expressed as % of cells.

We further studied the caspase-dependent cleavage of the nuclear protein PARP as a marker of canonical apoptosis. The p85 band, generated through proteolytic cleavage of p116 PARP by activated caspases, was clearly visible as early as 6 h after the treatment of A549 cells with PM01183 150 nM (Figure 3C). After 24 h of treatment, a considerable proportion of the PARP protein had already been cleaved by caspases, indicating that most of the cells were undergoing canonical apoptosis.

Finally, we analysed the onset of apoptosis using a commercially available solid-phase sandwich enzyme immunoassay that detects the cleavage of cytokeratin-18 (CK-18) by caspases as a sensitive and specific marker of early canonical apoptosis. Treatment with 150 nM PM01183 induced a marked increase of the apoptosis-related CK-18 Asp396 epitope in A549 cells. Moreover, simultaneous treatment with the pan-caspase inhibitor, Z-Vad-fmk, strongly reversed this effect (Figure 3D), which clearly indicates that the pro-apoptotic effect of PM01183 was dependent on caspase activity.

PM01183 shows a potent cytotoxic activity

The *in vitro* cytotoxicity of PM01183 was determined using a panel of 23 tumour cell lines that represent 11 relevant types of human cancer (Table 2). Most of the cell lines were very sensitive to PM01183 treatment, with GI_{50} values in the low nanomolar range (<10 nM). The panel average GI_{50} was 2.7 nM, with 22RV1, MiaPaCa-2, HS746T and MOLT4 cell lines showing the lowest GI_{50}, and IGROV-1, NCI-H23, RXF393 and HCT116 cell lines presenting the highest GI_{50} values.

We then performed xenograft studies to test whether the cytotoxicity of PM01183 translates into *in vivo* anti-tumour activity. NCI-H460 (lung), A2780 (ovary), HT29 (colon) and HGC-27 (gastric) cells were xenografted into the right flank of athymic *nu/nu* mice. Once the tumours reached *c.* 150 mm^3, the mice were randomized into groups of 10–15 mice each and either vehicle or PM01183 (0.18 $mg \cdot kg^{-1} \cdot day^{-1}$) was intravenously administered in three consecutive weekly doses. At the drug doses used in the experiment, no significant toxicity or body weight loss was observed in the treated animals (data not shown). As shown in Figure 4, PM01183 presented anti-tumour activity with a statistically significant inhibition of tumour growth in the four tested models.

Discussion

In the present work, we describe PM01183, a new synthetic tetrahydroisoquinoline alkaloid that induced DNA damage and apoptosis in a variety of cancer cell lines in the low nanomolar range and showed a potent anti-tumour activity in several human cancer cell lines and mouse xenograft models.

We first demonstrated that PM01183 was able to bind to a naked, 250 bp long PCR product containing multiple guanines spread over its whole length. This binding was dependent on the presence of the reactive hemiaminal moiety in the drug, as ET-745, a related compound devoid of the hydroxyl group, did not produce any band shifts at any of the concentrations tested. By using a highly sensitive and miniaturized fluorescence-based DNA melting assay, we observed that the preferred DNA triplets for PM01183 binding were AGC, CGG, AGG and TGG (the underlined guanine denoting the site of covalent adduct formation). These preferences are different from those of other DNA minor groove binders that alkylate DNA. For example, anthramycin selects AGA and AGG triplets (Pierce *et al.*, 1993), saframycins prefer GGG or GGC (Rao and Lown, 1992) while CC-1065 and derivatives (adozelesin,

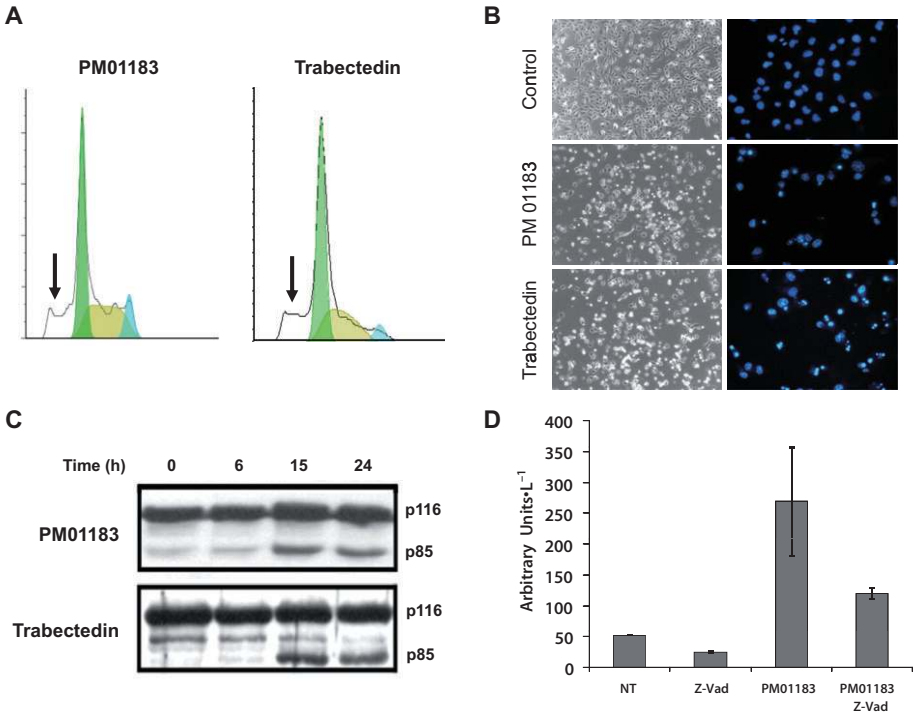

Figure 3

PM01183 induces apoptosis in living cells. (A) Flow cytometric DNA histograms showing sub-G1 peak induced by PM01183 and trabectedin (both drugs at 150 nM after 24 h exposure) in A549 cells. (B) Representative microphotographs of chromatin condensation of A549 cells without (Control) and after 24 h exposure to 150 nM of PM01183 or trabectedin. (C) Western blots of PARP in A549 cells after exposure to 150 nM of PM01183 and trabectedin at different time intervals. (D) Detection of cleaved cytokeratin-18 using the M30-Apoptosense kit in A549 cells after 24-hour exposure to PM01183 (150 nM) or not (NT).

bizelesin), as well as duocarmycin, prefer the minor groove of AT-rich regions (Baraldi *et al.*, 1999). On the other hand, preferential triplets for PM01183 binding were similar to those previously reported for trabectedin (TGG, CGG, AGC and GGC) (Marco *et al.*, 2006) and Zalypsis® (GGC and AGC) (Leal *et al.*, 2009). Nonetheless, although these three compounds share similar binding preferences, they differ in their kinetics of DNA adduct formation and in their degree of structural stabilization of the DNA double helix. PM01183 shows a higher affinity but gives rise to a lower duplex stabilization compared with trabectedin ($1/C_{50}$: 0.5 μM, data not shown; ΔT_m(max) ~20°C) (Casado *et al.*, 2008), which seems to indicate that PM01183 adducts are produced faster but they are slightly less effective in preventing strand separation, a process that must take place during transcription and replication. Whether these differences in affinity and DNA stabilization translate into differences in anti-tumour activities is not currently known in detail, although the present results appear to point in this direction.

A rationale for the reported binding preferences was provided by molecular modelling results which showed that a specific pattern of hydrogen bonds was necessary for both sequence recognition and PM01183 activation. The covalent complex with a representative oligonucleotide containing a central CGG triplet showed relatively minor structural distortions in the DNA molecule, the most significant being a widening of the minor groove in the region where the drug is bound and a distinct bending towards the major groove. Importantly, the guanine-bonded drug also establishes non-bonded (hydrophobic, van der Waals and electrostatic, including hydrogen bonding) interactions with surrounding nucleotides from both strands. A likely consequence, supported by the DNA melting results reported above, is that one or more PM01183-guanine adducts can hamper or prevent strand separation, thereby blocking replication and transcription forks. As a result, PM01183's behaviour could be akin to that of agents giving rise to true interstrand crosslinks (ICLs), such as mitomycin (Casado *et al.*, 2008). In this respect, it is of interest that ICL resolution is known to occur through the coordinated action of multiple DNA repair pathways, including homologous recombination, a process that gives rise to DSBs because both DNA strands are covalently modified and need to be incised.

Table 2
Cytotoxicity of PM01183 in a panel of 24 human cancer cell lines

	Cell line	PM01183 GI_{50} (nM)	Trabectedin GI_{50} (nM)
Prostate	PC3	1.2 ± 0.6	5.1 ± 2.4
	22RV1	0.3	1.1 ± 0.5
Pancreas	PANC-1	2.8 ± 1.4	8.4 ± 2.4
	MiaPaCa-2	1 ± 0.2	9.9 ± 2.1
Ovary	IGROV-1	9.7 ± 10	4.8 ± 3.1
	A2780	1.5 ± 0.4	3.1 ± 2.3
Lung	NCI-H460	1.5 ± 0.8	1.8 ± 0.8
	NCI-H23	5.3 ± 0.2	2.1 ± 1.3
	A549	1.3 ± 0.1	10.4 ± 7.6
Liver	SK-HEP-1	2.6 ± 1	4.7 ± 0.9
	HEPG2	3 ± 0.3	7.2 ± 1.3
Leukaemia	MOLT4	1.1 ± 0.04	1.6 ± 0.7
	K562	1.5 ± 1.8	3 ± 2.7
Kidney	RXF393	8.6 ± 0.5	3.3 ± 1
	CAKI-1	1.7 ± 1.1	5.9 ± 2
Stomach	HS746T	1 ± 3.1	9.9 ± 1.3
	HGC-27	2.8 ± 1.2	4.8 ± 1.2
Colon	LoVo	2 ± 1	1.5 ± 0.6
	HT29	2.4 ± 1	9.8 ± 4.3
	HCT-116	6.4 ± 3.7	4.9 ± 2.7
Breast	MDA-MB-231	3.4 ± 1.9	3.9 ± 4.2
	MCF-7	1.7 ± 0.6	2.6 ± 0.1
	BT-474	1.3 ± 0.4	4.6 ± 2

Values represent the mean ± SD of three different experiments.
GI_{50}, 50% growth inhibition.

When we tried to ascertain whether PM01183 treatment could induce DSB in human cancer cells, we confirmed that drug treatment at nanomolar concentrations did indeed give rise to a high proportion of DSB-positive cells with abundant γ-H2AX foci per cell. Moreover, the data presented here show that PM01183 induced an S-phase arrest at both low and high nanomolar concentrations. Altogether these findings indicate that some of the PM01183-DNA adducts are eventually transformed into DSB and induce an S-phase arrest by activation of the DNA replication checkpoints. Our data also showed that PM01183-induced cell death exhibited the characteristics of apoptosis, with chromatin condensation and cleavage of the caspase targets PARP-1 and CK-18.

These results are not surprising in light of similar findings recently reported for other DNA covalent minor groove binders. For example, trabectedin-DNA adducts trap the transcription-coupled-nucleotide excision repair (TC-NER) machinery, as it attempts to repair the lesion, at sites where those adducts have arrested RNA polymerase II (Pol II) (Erba *et al.*, 2001; Takebayashi *et al.*, 2001). In this action, the C-ring present in trabectedin, which protrudes from the DNA minor groove, has been proposed to interact with a key basic residue of the NER endonuclease XPG (Herrero *et al.*, 2006). Preliminary data support this view as fission yeast mutants defective in the orthologous Rad13 protein or tumour cells lacking XPG have been shown to be partially resistant to trabectedin (Takebayashi *et al.*, 2001; Herrero *et al.*, 2007). The formation of large ternary cytotoxic complexes (DNA–trabectedin–XPG) would result in DNA DSB during the S-phase and the repair of this type of DNA damage is known to require proteins from the homologous recombination machinery (Soares *et al.*, 2007; Tavecchio *et al.*, 2008). In contrast, the cytotoxic activity of Zalypsis®, which also induces DSB, is apparently not affected by NER deficiency as the formation of γ-H2AX foci was equally observed in models of NER-proficient and NER-deficient cells (Guirouilh-Barbat *et al.*, 2009). In this regard, it was recently found that PM01183 was three times less potent in NER-deficient cells compared with NER-proficient cells indicating that this compound could be also targeting TC-NER-dependent DNA repair (Aviles *et al.*, 2009). Trabectedin also induces the rapid and massive degradation of transcribing Pol II in various cancer cell lines (Aune *et al.*, 2008). Persistent Pol II degradation and lack of transcription would preclude the synthesis of essential cellular proteins. Similar alterations were observed after treatment of cancer cells with irofulven (Escargueil *et al.*, 2008). It is currently not clear whether PM01183 can also act on Pol II in a similar way.

When assayed in a panel of 23 cancer cell lines, PM01183 demonstrated a potent cytotoxic activity, with an average GI_{50} of 2.7 nM. All cell lines from the panel presented GI_{50} values lower than 10 nM. Other DNA minor groove binders of the tetrahydroisoquinoline family, including trabectedin, Zalypsis®, jorumycin, renieramycins and saframycins, have been previously shown to possess strong cytotoxic activity, with GI_{50}s also in the low nanomolar range (Arai *et al.*, 1980; Oku *et al.*, 2003; Lane *et al.*, 2006; Leal *et al.*, 2009). The *in vitro* cytotoxicity of PM01183 translated well into *in vivo* antitumour activity in four xenograft models of human cancer. We assayed the maximum tolerated dose of the drug with no toxic effects to the animals. PM01183 showed clear antineoplastic activity against xenograft models of different tissue types.

In summary, we have demonstrated highly potent *in vitro* and *in vivo* anti-cancer activities of PM01183. This agent exerts its anti-cancer effects

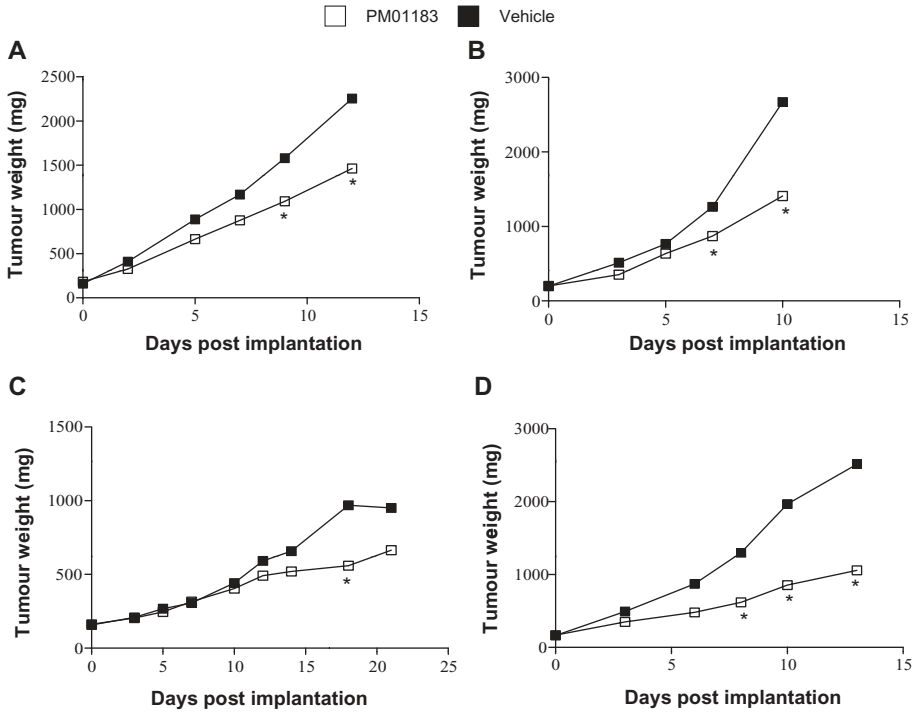

Figure 4

In vivo anti-tumour activity of PM01183. Treatment with PM01183 results in tumour growth inhibition in NCI-H460 lung (A), A2780 ovarian (B), HT29 colon (C) and HGC-27 gastric (D) xenograft models compared with vehicle-treated animals. Treatments started at a tumour volume size of *c.* 150 mm^3 and were intravenously administered in three cycles of three consecutive weekly doses at 0.18 $mg \cdot kg^{-1}$. Each point represents the median value ($n = 10$); *$P < 0.05$.

through the covalent modification of guanines in the DNA minor groove that eventually give rise to DNA DSB, S-phase arrest and apoptosis in cancer cells. These encouraging results support its development as a novel anti-cancer agent in a wide spectrum of clinical settings.

Acknowledgements

The authors thank Beatriz de Castro, Guillermo Tarazona Ramos, Maribel Cercenado Mansilla, Patricia Martinez Rivas and Sofia Cascajares for their excellent technical assistance. This work was funded by PharmaMar SA.

Conflicts of interest

Alberto Domingo and Federico Gago have received a Research Grant from PharmaMar JFM Leal, M Martinez-Diez, V Moneo, MJ Guillen Navarro, P Aviles, C Cuevas, LF Garcia Fernandez and CM Galmarini are employees and shareholders of PharmaMar SA.

References

Arai T, Takahashi K, Nakahara S, Kubo A (1980). The structure of a novel antitumor antibiotic, saframycin A. Experientia 36: 1025–1027.

Aune GJ, Takagi K, Sordet O, Guirouilh-Barbat J, Antony S, Bohr VA *et al.* (2008). Von Hippel-Lindau-coupled and transcription-coupled nucleotide excision repair-dependent degradation of RNA polymerase II in response to trabectedin. Clin Cancer Res 14: 6449–6455.

Aviles PM, Galmarini CM, Cuevas C, Guillen MJ, Frapolli R, Uboldi S *et al.* (2009). Mechanism of action and antitumor activity of PM01183. In: Proceedings of the 100th Annual Meeting of the American Association for Cancer Research, AACR: Denver, CO, Abstract 2679.

Baraldi PG, Cacciari B, Guiotto A, Romagnoli R, Zaid AN, Spalluto G (1999). DNA minor-groove binders: results and design of new antitumor agents. Farmaco 54: 15–25.

Casado JA, Rio P, Marco E, Garcia-Hernandez V, Domingo A, Perez L *et al.* (2008). Relevance of the Fanconi anemia pathway in the response of human cells to trabectedin. Mol Cancer Ther 7: 1309–1318.

Case DA, Cheatham III, TE, Darden T, Gohlke H, Luo R, Merz Jr., KM *et al*. (2005). The Amber biomolecular simulation programs. J Comput Chem 26: 1668–1688.

David-Cordonnier MH, Gajate C, Olmea O, Laine W, Iglesia-Vicente J, Perez C *et al*. (2005). DNA and non-DNA targets in the mechanism of action of the antitumor drug trabectedin. Chem Biol 12: 1201–1210.

Erba E, Bergamaschi D, Bassano L, Damia G, Ronzoni S, Faircloth GT *et al*. (2001). Ecteinascidin-743 (ET-743), a natural marine compound, with a unique mechanism of action. Eur J Cancer 37: 97–105.

Escargueil AE, Poindessous V, Soares DG, Sarasin A, Cook PR, Larsen AK (2008). Influence of irofulven, a transcription-coupled repair-specific antitumor agent, on RNA polymerase activity, stability and dynamics in living mammalian cells. J Cell Sci 121: 1275–1283.

Garcia-Nieto R, Manzanares I, Cuevas C, Gago F (2000). Bending of DNA upon Binding of Ecteinascidin 743 and Phthalascidin 650 Studied by Unrestrained Molecular Dynamics Simulations. J Am Chem Soc 122: 7172–7182.

Guan Y, Sakai R, Rinehart K, Wang AH (1993). Molecular and crystal structures of ecteinascidins: potent antitumor compounds from the Caribbean thnicate ecteinascidia turbinata. J Biomol Struct Dyn 10: 793–818.

Guirouilh-Barbat J, Antony S, Pommier Y (2009). Zalypsis (PM00104) is a potent inducer of gamma-H2AX foci and reveals the importance of the C ring of trabectedin for transcription-coupled repair inhibition. Mol Cancer Ther 8: 2007–2014.

Herrero A, Marco E, García-Hernández V, Martín-Castellanos C, Domingo A, Alvarez E *et al*. (2007). Resilience of the cytotoxic effects of Zalypsis® (pm00104) to the lack of a functional nucleotide excision repair system. In: American Association for Cancer Research Annual Meeting. Proceedings: Los Angeles, CA, Abstract 1537.

Herrero AB, Martin-Castellanos C, Marco E, Gago F, Moreno S (2006). Cross-talk between nucleotide excision and homologous recombination DNA repair pathways in the mechanism of action of antitumor trabectedin. Cancer Res 66: 8155–8162.

Kishi K, Yazawa K, Takahashi K, Mikami Y, Arai T (1984). Structure-activity relationships of saframycins. J Antibiot (Tokyo) 37: 847–852.

Lane JW, Estevez A, Mortara K, Callan O, Spencer JR, Williams RM (2006). Antitumor activity of tetrahydroisoquinoline analogues 3-epi-jorumycin and 3-epi-renieramycin G. Bioorg Med Chem Lett 16: 3180–3183.

Leal JF, Garcia-Hernandez V, Moneo V, Domingo A, Bueren-Calabuig JA, Negri A *et al*. (2009). Molecular pharmacology and antitumor activity of Zalypsis in several human cancer cell lines. Biochem Pharmacol 78: 162–170.

Manzanares I, Cuevas C, Garcia-Nieto R, Marco E, Gago F (2001). Advances in the chemistry and pharmacology of ecteinascidins, a promising new class of anti-cancer agents. Curr Med Chem Anticancer Agents 1: 257–276.

Marco E, David-Cordonnier MH, Bailly C, Cuevas C, Gago F (2006). Further insight into the DNA recognition mechanism of trabectedin from the differential affinity of its demethylated analogue ecteinascidin ET729 for the triplet DNA binding site CGA. J Med Chem 49: 6925–6929.

Moore BM, Seaman FC, Hurley LH (1997). NMR-based model of an Ecteinascidin 743-DNA adduct. J Am Chem Soc 119: 5475–5476.

Negri A, Marco E, Garcia-Hernandez V, Domingo A, Llamas-Saiz AL, Porto-Sanda S *et al*. (2007). Antitumor activity, X-ray crystal structure, and DNA binding properties of thiocoraline A, a natural bisintercalating thiodepsipeptide. J Med Chem 50: 3322–3333.

Oku N, Matsunaga S, van Soest RW, Fusetani N (2003). Renieramycin J, a highly cytotoxic tetrahydroisoquinoline alkaloid, from a marine sponge Neopetrosia sp. J Nat Prod 66: 1136–1139.

Pabo CO, Sauer RT (1984). Protein-DNA recognition. Annu Rev Biochem 53: 293–321.

Pierce JR, Nazimiec M, Tang MS (1993). Comparison of sequence preference of tomaymycin- and anthramycin-DNA bonding by exonuclease III and lambda exonuclease digestion and UvrABC nuclease incision analysis. Biochemistry 32: 7069–7078.

Pommier Y, Kohlhagen G, Bailly C, Waring M, Mazumder A, Kohn KW (1996). DNA sequence- and structure-selective alkylation of guanine N2 in the DNA minor groove by ecteinascidin 743, a potent antitumor compound from the Caribbean tunicate Ecteinascidia turbinata. Biochemistry 35: 13303–13309.

Rao KE, Lown JW (1992). DNA sequence selectivities in the covalent bonding of antibiotic saframycins Mx1, Mx3, A, and S deduced from MPE.Fe(II) footprinting and exonuclease III stop assays. Biochemistry 31: 12076–12082.

Reddy BS, Sharma SK, Lown JW (2001). Recent developments in sequence selective minor groove DNA effectors. Curr Med Chem 8: 475–508.

Rinehart K, Holt TG, Fregeau NL, Stroh JG, Keifer PA, Sun F *et al*. (1990). Ecteinascidins 729, 743, 745, 759A, 759B and 770: potent antitumor agents from the Caribean tunicate Ecteinascidia turbinata. J Org Chem 55: 4512–4515.

Rohs R, West SM, Sosinsky A, Liu P, Mann RS, Honig B (2009). The role of DNA shape in protein-DNA recognition. Nature 461: 1248–1253.

Seaman FC, Hurley LH (1998). Molecular basis for the DNA sequence selectivity of ecteinascidin 736 and 743: evidence for a dominant role of direct readout via hydrogen bonding. J Am Chem Soc 120: 13028–13041.

Soares DG, Escargueil AE, Poindessous V, Sarasin A, de Gramont A, Bonatto D *et al*. (2007). Replication and homologous recombination repair regulate DNA double-strand break formation by the antitumor alkylator ecteinascidin 743. Proc Natl Acad Sci USA 104: 13062–13067.

Susbielle G, Blattes R, Brevet V, Monod C, Kas E (2005). Target practice: aiming at satellite repeats with DNA minor groove binders. Curr Med Chem Anticancer Agents 5: 409–420.

Takebayashi Y, Pourquier P, Zimonjic DB, Nakayama K, Emmert S, Ueda T *et al*. (2001). Antiproliferative activity of ecteinascidin 743 is dependent upon transcription-coupled nucleotide-excision repair. Nat Med 7: 961–966.

Tavecchio M, Simone M, Erba E, Chiolo I, Liberi G, Foiani M *et al*. (2008). Role of homologous recombination in trabectedin-induced DNA damage. Eur J Cancer 44: 609–618.

Supporting information

Additional Supporting Information may be found in the online version of this article:

Figure S1 Chemical structures of trabectedin (ET-743) and ET-745.
Table S1 Sequences of the ds-oligonucleotides used in the DNA melting assays.
Table S2 Cell cycle perturbations after 12 h exposure of tumour cells to PM01183.

Please note: Wiley-Blackwell are not responsible for the content or functionality of any supporting materials supplied by the authors. Any queries (other than missing material) should be directed to the corresponding author for the article.